the intensity of Mo–P coordination increases, and the Mo–C/O bonds slightly shift to a lower radical distance. These observations should result from the lattice distortion by P incorporation. Indeed, they clearly confirm the presence of P–Mo bonds in P-Mo_2C@C and the direct interaction between the dopant and carbide. Additionally, P K-edge and C K-edge X-ray absorption near edge structure (XANES) spectra are also recorded. **Figure 1(c)** depicts the P K-edge XANES spectra of P-Mo_2C@C, and the XANES spectra of MoP is also replotted from the reference. Except for the sharp peak around 2153 eV related with phosphates, the broad feature at the pre-edge region (around 2145 eV) further indicates the formation of Mo–P species, showing the increasing trend corresponding to the enhanced Mo–P coordination (**Fig. 1(b)**). The C K-edge XANES results are presented in **Fig. 1(d)** in which pronounced C=C π* and C–C σ* resonances located at 285 and 292 eV can be observed, respectively. The additional peak and shoulder at 288 eV and 284 eV respectively should be assigned to typical features of Mo2C. Another shoulder around 287 eV is typically associated to carbon bonded with nitrogen and phosphorus, demonstrating the co-doping of N and P into the carbon matrix. Noticeably, the P-Mo_2C@C and Mo_2C@C samples display slight changes in the C K-edge XANES profiles, which indicates the negligible influence on the carbon matrix after varied P-doping.

In summary, controlled P-doping was developed to effectively optimize the electronic configuration and HER activity of Mo_2C electrocatalysts. Remarkably, P-doping into Mo_2C can increase the electron density around the Fermi level of Mo_2C, leading to weakened Mo–H bonding promoting HER kinetics. The synergy of electron transfers into the anti-bonding orbitals of Mo–H and steric hindrance of H atoms on P-doped sites is responsible for the effectively weakened Mo–H. This work opens up a new opportunity to develop efficient noble-metal-free catalysts. (Reported by Yan-Gu Lin)

This report features the work of Zhangping Shi and his co-workers published in Energy Environ. Sci. ***10****, 1262 (2017).*

TLS 01C1 SWLS – EXAFS
TLS 16A1 BM – Tender X-ray Absorption, Diffraction
TLS 20A1 BM – (H-SGM) XAS

- XANES, EXAFS
- Materials Science, Chemistry, Condensed Matter Physics, Environmental and Earth Science

Reference

1. Z. Shi, K. Nie, Z.-J. Shao, B. Gao, Hu. Lin, H. Zhang, B. Liu, Y. Wang, Y. Zhang, X. Sun, X.-M. Cao, P. Hu, Q. Gao, and Y. Tang, Energy Environ. Sci. **10**, 1262 (2017).

Voltammetric Enhancement of Li-ion Conduction in Al-Doped $Li_{7-x}La_3Zr_2O_{12}$ Solid Electrolyte

Cyclic voltammetry has served as a tool to accelerate the Li-ion mobility within a garnet-phase solid electrolyte, Al-doped $Li_{7-x}La_3Zr_2O_{12}$; the modification of the local ionic arrangements has been studied by refinement of neutron powder diffraction (NPD) ex situ and correlated with the results of X-ray absorption near-edge spectra (XANES).

A cutting-edge Li-ion battery (LIB) utilizes liquid or organic-based electrolytes. Several challenges and safety issues restrict their use in high-temperature operation and small-scale devices. Solid-state Li-ion conductors are promising alternatives to liquid-based LIB electrolytes, mitigating the safety issues of dendritic Li growth.[1] Among Li-ion conducting materials, $Li_7La_3Zr_2O_{12}$ (LLZO), possessing a garnet-type crystal structure, is of particular interest for application as a solid LIB electrolyte because of its suitable ionic conductivity, chemical stability in a wide potential range and ease of scaling for industrial applications.[2] LLZO can crystallize in cubic or tetragonal symmetry phases depending on the conditions of synthesis. Cubic LLZO possesses space group symmetry $Ia\bar{3}d$ with La, Zr and O atoms located at 24*c*, 16*a* and 96*h* sites, respectively, whereas Li occupies both 24*d* tetrahedral and 96*h* octahedral sites.[3] Tetragonal LLZO possesses space group symmetry $I4_1/acd$ with La, Zr and O atoms located at 8*b* (and 16e), 16*c* and 32*g* sites, respectively. The conductivity of tetragonal LLZO is about 1/100 that of cubic LLZO; doping with Al, which preferably occupies the 24*d* site, provides a method to stabilize the more favorable cubic LLZO phase.

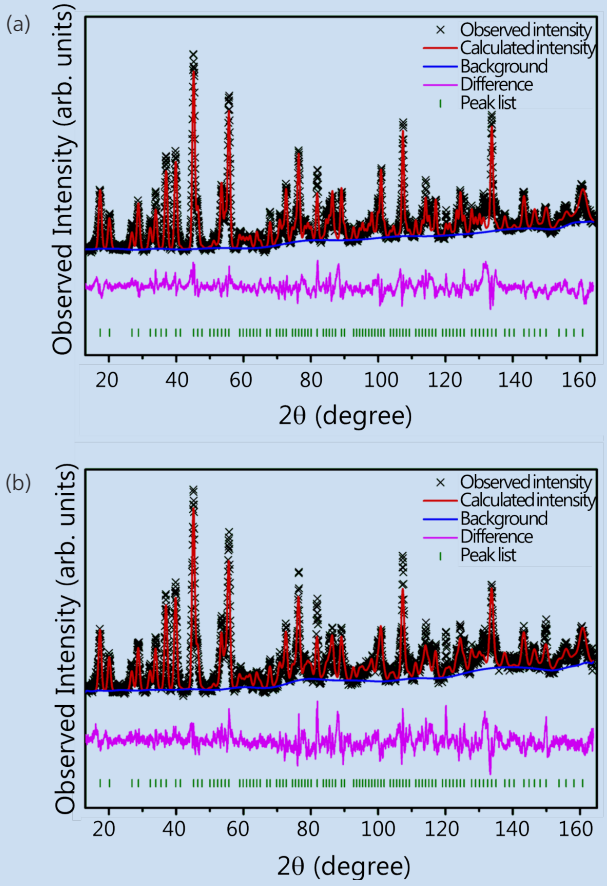

Fig. 1: Rietveld refinement profiles for LLZO using neutron powder-diffraction data (a) before and (b) after voltammetric treatment. [Reproduced from Ref. 4]

The mechanism of Li-ion conduction in LLZO has been studied with a focus on the bottlenecks. In this article, the study[4] by Yu-Ting Chen (National Taiwan University), Ru-Shi Liu (National Taiwan University) *et al.* is reported; a voltammetric treatment was used to investigate the electrochemical behavior of Al-doped LLZO. Instead of a non-continuous current, a smoothly evolving potential was applied to LLZO. After that treatment, the ionic conductivity of LLZO became much enhanced without significantly increasing the electronic conductivity. Subsequent characterizations were conducted to deduce the mechanism of such an increment in ionic conduction without affecting the electronic migration. Systems with both Li (non-blocking) and Au (blocking) electrodes were utilized in the electrochemical analyses, but the current report highlights only the non-blocking results from the published data.

Al-doped LLZO was synthesized through a solid-state reaction. The LLZO was ground into powder (#200 mesh) and then uniaxially pressed into pellets (diameter 12 mm) at 1734 MPa. The pellets were polished repeatedly to obtain a mirror-like surface and then assembled in a Swagelok cell using the Li | LLZO | Li configuration for further study. A complete low-frequency semicircle resulting from charge transfer of Li ions at the interface between LLZO and Li metal presents the reversible nature in such system. The total ionic conductivity of LLZO was increased from 3.4×10^{-4} S/cm before voltammetric treatment to 1.2×10^{-3} S/cm afterward.

Rietveld refinement profiles for the LLZO before and after voltammetric treatment are shown in **Fig. 1** using NPD data. Before voltammetric treatment, the LLZO had fully occupied La, Zr and O sites and ~4.98 Li atoms per formula unit; after that treatment, the total Li content increased to ~5.55 Li atoms per formula unit, probably as a result of the inclusion of Li ions through the oxidation of Li metal during the voltammetric treatment.

The phenomenon is also present in XANES, through the energies at the absorption edge being smaller than for the corresponding oxide standard, shown in **Fig. 2**. Nevertheless, the chemical environment of LLZO differs from that of the corresponding oxides

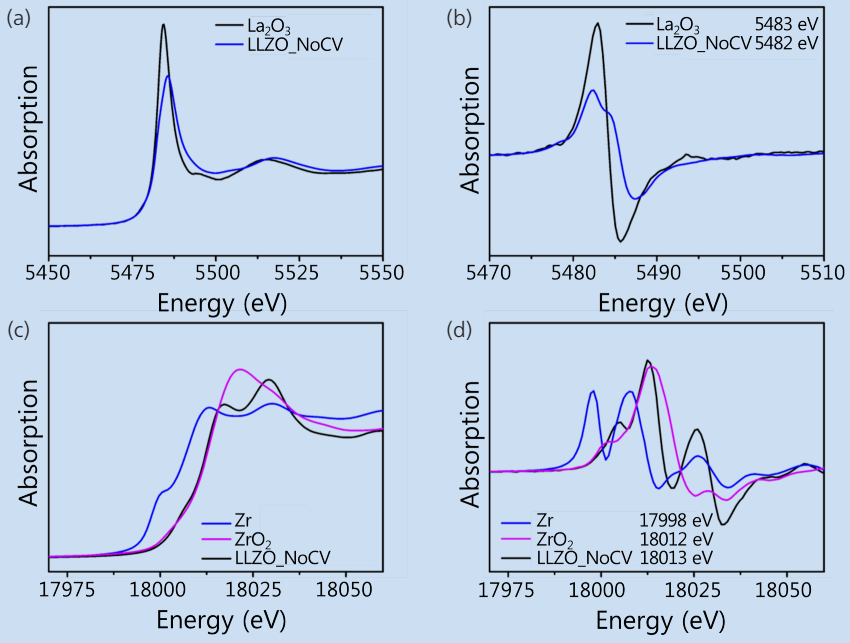

Fig. 2: XANES data at (a) La L3 and (c) Zr K-edge and first derivative of data at (b) La L3 and (d) Zr K-edge [Reproduced from Ref. 4]

as a result of the three distinct cations, complicating the determination of the chemical state according to the pure oxide reference spectra. Importantly, an increased binding energy of both Zr and La following voltammetric treatment was found, which might have arisen from the inclusion of additional Li ions. (Reported by Ru-Shi Liu, National Taiwan University)

This report features the work of Ru-Shi Liu and his co-workers published in J. Phys. Chem. C ***121****, 15565 (2017).*

ANSTO-TG1 ECHINDA – High-resolution Powder Diffractometer
TLS 01C1 SWLS – EXAFS
TLS 17C1 W200 – EXAFS

- XANES, Oxidation State
- Neutron Powder Diffraction, Crystal Structure, Materials Chemistry

References

1. S. Yu, R. D. Schmidt, R. Garcia-Mendez, E. Herbert, N. J. Dudney, and J. B. Wolfenstine, J. Sakamoto, and D. J. Siegel, Chem. Mater. **28**, 197 (2016).
2. S. Song, B. Yan, F. Zheng, H. M. Duong, and L. Lu, Solid State Ionics **268**, 135 (2014.)
3. J. Awaka, A. Takashima, K. Kataoka, N. Kijima, Y. Idemoto, and J. Akimoto, Chem. Lett. **40**, 60 (2011).
4. Y. T. Chen, A. Jena, W. K. Pang, V. K. Peterson, H. S. Sheu, H. Chang, and R. S. Liu, J. Phys. Chem. C **121**, 15565 (2017).

Molecular Design Drives Solar-Hydrogen Conversion

A rational molecular design of polymer heterojunctions is an effective strategy to benefit the exciton dissociation or light-harvesting ability for efficient conversion of solar energy.

The key to solar-hydrogen conversion (SHC) is to develop an ideal photocatalyst with not only an efficient and stable ability for hydrogen production driven with visible light but also a nontoxic and terrestrially abundant elemental composition for promising industrial application. The photocatalysts developed so far are mainly inorganic semiconductors, but the necessity of noble or toxic metals might be a serious hindrance to a large-scale industrial application of those inorganic semiconductors. In contrast, organic semiconductors are more intriguing for photocatalytic applications in terms of terrestrial abundance and environmental benignity, but most organic semiconductors have shown poor photocatalytic SHC efficiencies for three well known reasons: first, the large band gaps limit their harvest to a small portion of visible light; second, unlike free Wannier excitons photogenerated in inorganic semiconductors, photoexcitation of an organic semiconductor typically generates Frenkel excitons with a large exciton binding energy, hence small dissociation probability, resulting in serious charge recombination; third, because of a lack of catalytic reaction sites on the surface of the semiconductor, even if the charge carriers survive recombination, they can contribute only to surface water reduction with a small probability. The further design of organic photocatalysts toward a highly efficient photocatalytic SHC is hence crucial.

In this work, Shaohua Shen and his collaborators reported polymer heterojunction (PHJ) photocatalysts consisting of polymers in the polyfluorene family (PF) and graphitic carbon nitride (g-C_3N_4) for an efficient SHC.[1] A strategy of molecular design was executed to achieve an improved exciton dissociation and extended light absorption of PHJ photocatalysts for highly efficient photocatalytic SHC. The authors applied synchrotron-based X-ray adsorption techniques at **TLS 20A1** and **TLS 16A1** to clarify the intermolecular interactions between electron-rich aromatic rings of the PF and electron-deficient heptazine rings of g-C_3N_4.

To acquire profound insight into the electron transfer processes in these PHJ, X-ray absorption near-edge structure (XANES) spectra of the C-, N- and S-edges of the samples as prepared were recorded both in darkness and under illumination. The S K-edge spectra, which probes S 3*p* unoccupied states, is displayed in **Fig. 1(a)**. It can be observed that there is no spectral difference in pure PFBT with or without illumination, whereas the peak intensity of PFBT/CN decreases under illumination. Specifically, the electron transfer in PFBT/CN differs from that in PFO/CN or PCzF/CN, because of the introduction of the benzothiadiazole unit containing a S atom. Note that the N–C=N bonds exist only in g-C_3N_4; the C and N K-edge XANES spec-